ELSEVIER

S0032-3861(96)00393-X

Polymer Vol. 37 No. 25, pp. 5639–5647, 1996
Copyright © 1996 Elsevier Science Ltd
Printed in Great Britain. All rights reserved
0032-3861/96/$15.00+0.00

Drawing and orientation development of aromatic polyesters containing terphenyl units in the main chain and aliphatic side chains

A. Bruggeman* and J. A. H. M. Buijs
TNO Institute of Industrial Technology, PO Box 6031, 2600 JA Delft, The Netherlands
(Received 27 November 1995; revised 30 January 1996)

A range of aromatic polyesters containing terphenyl units in the main chain and alkyl side chains have been investigated with respect to their structure and orientation development. As-cast films showed a layered structure: layers of the main chains were preferentially organized parallel to the film surface. Upon drawing of these films, the structure changed to a fibre-symmetric one, as was proven by wide-angle X-ray diffraction (WAXD). Possible morphologies, which are based on WAXD and Raman data, are proposed. The development of the orientation with draw ratio appeared to be extremely efficient, even more efficient than that according to the affine deformation model. This was explained by the fact that the affine model assumes thin rods, whereas in reality, the orientation of units with a considerable thickness takes place. Copyright © 1996 Elsevier Science Ltd.

(Keywords: rigid-rod polymer; aromatic polyester; orientation)

INTRODUCTION

Rigid-rod polymers are mainly interesting because of their high mechanical stiffness and strength. Some other favourable properties can be their low melt viscosity in the case of thermotropic behaviour, and a low or negative coefficient of thermal expansion. To improve the generally poor processability, side chains can be attached to the main chains. Much effort has been devoted to a better understanding of the phase behaviour and the structure of these polymers. Several rigid-rod polymers with side chains are known to have a layered structure[1–3]. In films of a polyester with a poly(*p*-phenylene terephthalate) backbone and dodecyloxy side chains, denoted as PTA12HQ, the main chains were organized in layers, with planes of the main-chain layers being parallel to the film surface[2,4,5]. Drawing of this film induced orientation of the main chains, while the main-chain layers retained most of their ordering parallel to the film surface, as was proven by wide-angle X-ray diffraction (WAXD). A virtually maximum orientation, inferred from the tensile modulus, could be achieved[4] by drawing up to a draw ratio, λ, of 6. The polymers described in this present paper are polyesters with stiff terphenyl units in the backbone, and hexyl or dodecyl side chains. The structure of films of these polyesters was investigated, and the orientation development by drawing was studied by using WAXD, and compared to the orientation parameters determined by using Raman spectroscopy. Finally, the orientation development is discussed by comparing it with the affine deformation model and the two-dimensional version of this model.

* To whom correspondence should be addressed

EXPERIMENTAL

Materials

The polymers used in this study were synthesized at the TNO Institute of Industrial Technology, according to a procedure described by Tiesler and coworkers[6,7]. The chemical structures are depicted in *Scheme 1*. The polyesters are denoted as PES*x.y*/C*n*, with *x* the number of phenylene rings in the diacid monomer, *y* the number of phenylene rings in the dihydroxy monomer, and *n* the number of carbon atoms in the side chain. For comparison, the structure of PTA12HQ is also shown. Some properties of the synthesized polymers are listed in *Table 1*. Some of the polymers showed multiple melting peaks in differential scanning calorimetry (d.s.c.) studies, including a liquid crystalline phase.

Film casting and drawing

Films were prepared by casting from an isotropic solution of 3–6 wt% polymer in chloroform. Prior to the film casting, the solution was filtered through a Teflon filter (Millipore, 5 μm pore size) in order to remove any dust particles. Solutions were cast on to a glass plate at room temperature with a 1000 μm blade. The solvent was evaporated and films with a uniform thickness of 30 ± 2 μm were obtained.

Oriented films were obtained by drawing cast films in an oven or on a hot shoe, at ca. 200°C for PES1.3/C12 and ca. 270°C for PES1.3/C6 and PES3.3/C6. The sample was heated by passing preheated dry nitrogen gas through the oven. The drawing speed was 2 cm min^{-1}, with the specimen length and width before drawing being ca. 5 and 1 cm, respectively. The draw

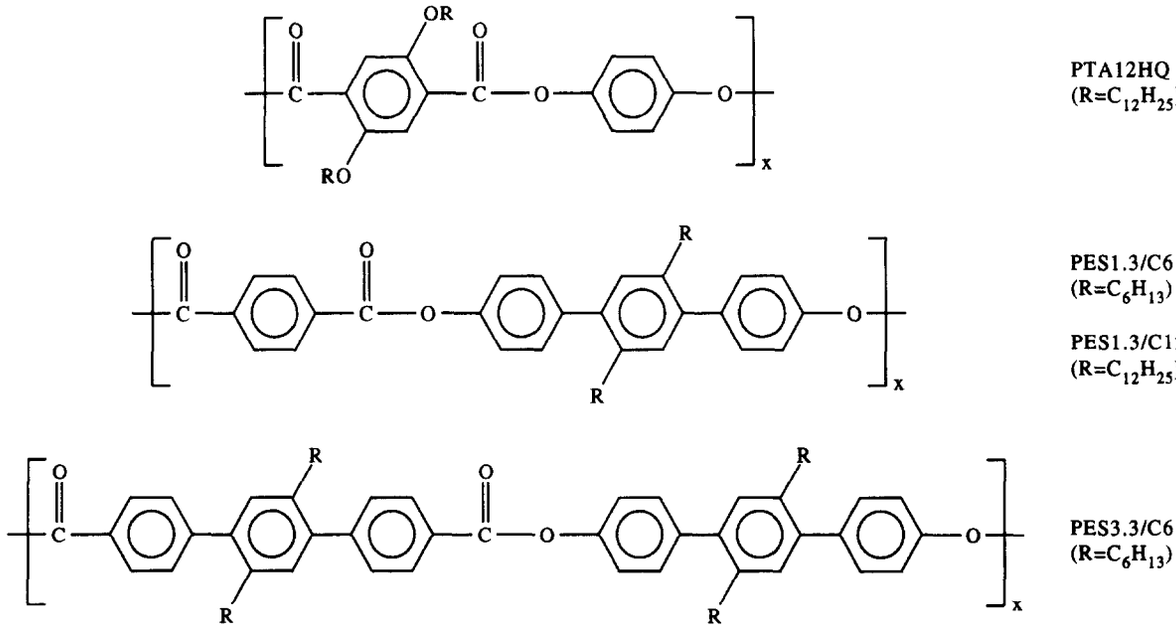

Scheme 1

ratio, λ, was determined from the length increase of the central part of the film specimen.

Wide angle X-ray diffraction (WAXD)

Film diffractograms were recorded in transmission mode by using Ni-filtered CuKα radiation (flat film, sample to film distance of 6 cm). The azimuthal intensity distribution $I(\phi)$ of the most intense equatorial reflection, i.e. 100, was established with an ENRAF-Nonius densitometer, via radial scans with a varying step size of 1 to 5 degrees. The intensity profile was corrected for the background by subtracting the (constant) intensity level at high azimuthal angles. The resulting experimental profiles are convolutions of the orientation distribution and the scattering of a perfectly aligned system[8]. The profile of a perfectly aligned system is not known, but the narrowest peak obtained experimentally represents an upper limit of this profile, while its lower limit is set by a width of 0°. The experimentally determined profile has to be deconvoluted in order to obtain the orientation distribution. As a first approach, 0° can be taken for the width of the perfectly aligned system. The second moment of the orientation distribution $\langle P_2 \rangle = (3\langle \cos^2 \theta \rangle - 1)/2$, is generally used for quantifying the degree of orientation. This orientation parameter is related to the (deconvoluted) intensity profile by the following relationship:

$$\langle \cos^2 \theta \rangle = \frac{\int_{-\pi/2}^{\pi/2} I(\phi) \cos^2 \phi \sin \phi \, d\phi}{\int_{-\pi/2}^{\pi/2} I(\phi) \sin \phi \, d\phi} \qquad (1)$$

In this work, $\langle \cos^2 \theta \rangle$, and thus $\langle P_2 \rangle$, were calculated by a numerical integration of the intensity profile $I(\phi)$ by using equation (1).

RESULTS AND DISCUSSION

Film structure by WAXD

The X-ray diffractograms of cast films of PES1.3/C6, PES1.3/C12, and PES3.3/C6 showed a layered organization similar to the one found for PTA12HQ, but are less ordered. There is a clear difference in the diffractograms with the beam perpendicular and parallel to the film surface, respectively. This is illustrated in *Figure 1* for PES1.3/C12. *Figure 2* shows the equatorial scans obtained from *Figure 1*. In the photographs taken with the beam parallel to the surface the appearance of equatorial reflections points to a structure where layers formed by the main chains are lying preferentially parallel to the surface of the film. The broad equatorial reflection at around $2\theta = 20°$ ($d = 4.3$–4.8 Å) corresponds to an ill-defined distance between the main chains in these layers[2,5]. No higher-order reflections were observed. Tiesler and coworkers[6,7] found similar reflections in their powder diffractograms of PES1.3/C6. *Table 2* lists the characteristic distances found in the drawn films. Data for PTA12HQ, taken from Damman *et al.*[5], have been included in this table.

Table 1 Some properties of the synthesized polymers

Polymer	$[\eta]^a$ (dl g^{-1})	$M_w/M_n{}^b$	ρ^c (g cm^{-3})	$T_{transitions}{}^d$ (°C)
PES1.3/C6	4.5	3.6	1.10	352/368
PES1.3/C12	3.9	2.7	1.05	305/367
PES3.3/C6	4.3	3.6	1.06	343

[a] In chloroform at 25°C
[b] From gel permeation chromatography
[c] Of cast films, measured in a density gradient column: NaBr/KI/IPA/H_2O, at 23°C
[d] Peak temperatures measured by d.s.c., 20°C min^{-1}, under N_2

It is interesting to compare the X-ray spacings of the different polymers in terms of both the side-chain length and the substitution density of the side chains. In *Figure 3* the first equatorial spacings are plotted against the number (n) of CH_2 units in a side chain divided by the 'repeat distance' l between the side chains. For PTAnHQ (dotted lines in *Figure 3*) the oxygen in the side chain has been counted as a CH_2 unit. Plotting against the parameter n/l is more appropriate than using the weight fractions of side chains, because the latter is

Table 2 Characteristic WAXD spacings of drawn films, recorded with the X-ray beam parallel to the surface of the film[a]

	Equatorial spacings (Å)			Meridional spacings (Å)			
Polymer	1st	2nd	3rd	1st	2nd	3rd	4th
PES1.3/C6	13.1 (s)	7.1 (w)	4.3 (s)	23.2 (w)	11.0 (w)	7.0 (w)	5.2 (s)
PES1.3/C12	18.9 (s)	10.0 (w)	4.5 (s)	–	–	5.3 (s)	
PES3.3/C6	14.9 (s)	7.3 (w)	4.8 (s)	–	–	4.9 (s)	3.5 (w)
PTA12HQ A	21.0 (s)	10.5 (s)	7.0 (s)	–	–	–	–
B	15.2 (s)	7.6 (s)	5.1 (s)	12.2 (s)	6.3 (w)	4.1 (w)	2.2 (w)

[a] s = strong reflection; w = weak reflection

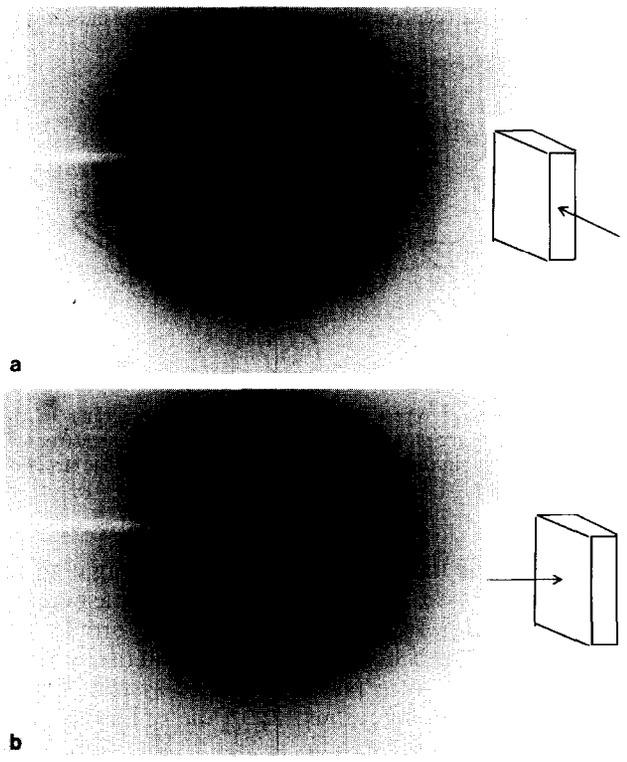

Figure 1 Flat-plate X-ray diffractograms of as-cast films of PES1.3/C12, with the X-ray beam (a) parallel to, and (b) perpendicular to the film surface, as indicated on the figures; sample-to-film distance is 6 cm

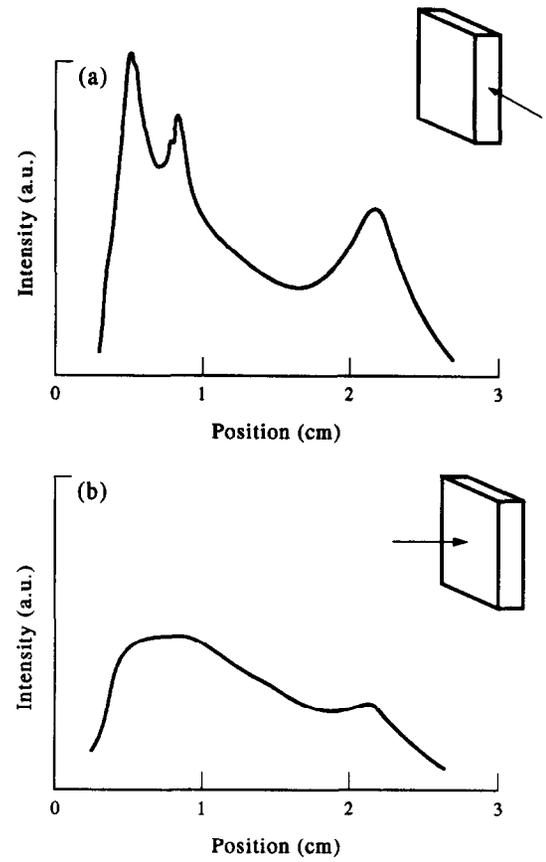

Figure 2 Equatorial scans of as-cast films of PES1.3/C12 (from the photographs shown in *Figure 1*). The direction of the X-ray beam is (a) parallel to, and (b) perpendicular to the film surface, as indicated on the figure

affected by the weight of the main chain, while here it concerns only spatial arrangements. Compared to the data for PTAnHQ, the polymers studied in this present paper show systematically larger spacings at comparable side-chain densities. As the overall density of all of the polymers listed in *Table 1* does not differ significantly, a possible explanation for the differences might be that the polymers under investigation here have thicker main-chain layers than PTAnHQ.

The X-ray spacings were not significantly altered by drawing of the films, nor by annealing. The maximum attainable draw ratio was ca. 4 for PES1.3/C12, and 3 for PES1.3/C6 and PES3.3/C6. Further drawing, at any temperature, caused breaking of the film. Apart from the main chains, it is probable that the length and density of side chains also play a role in the maximum attainable draw ratio. It was confirmed that the molecular weight was not the limiting factor for the achieved draw ratios.

Figure 4 illustrates the development of orientation upon drawing of a PES1.3/C6 film. The other two polyesters showed similar patterns. The sharpening of the equatorial reflections shows that the main chains were aligned along the draw direction very effectively. The meridional streaks indicate that no lateral correlation between the main chains exists.

Recordings taken with the beam parallel and perpendicular to the film surface both showed the same pattern, while recordings with the beam parallel to the draw direction revealed isotropic rings for all three polyesters (*Figure 5* shows this for PES1.3/C6), which indicates that as a result of drawing the structure changed from a planar to a cylindrically symmetric arrangement. The WAXD results are schematically drawn in *Figure 6*. This behaviour is remarkably different to that of the polyester PTA12HQ, which retained its planar structure after drawing[4,5]. The change to a

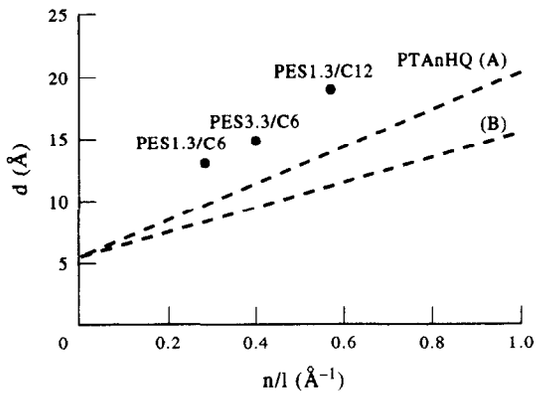

Figure 3 X-ray spacings of the first equatorial reflection of all three polyesters, and of PTAnHQ[1] (dotted lines, modifications A and B, respectively; data from ref. 1) as a function of the 'side chain parameter' n/l (see text for details)

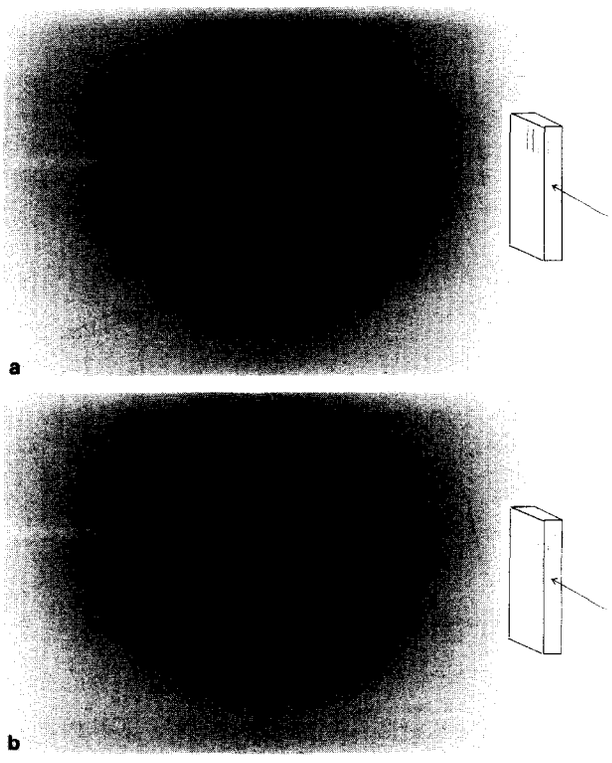

Figure 4 Flat-plate X-ray diffractograms of PES1.3/C6 films with a draw ratio λ of (a) 2.2 and (b) 3.0; the orientation direction is vertical, the X-ray beam is directed parallel to the film surface, and the sample-to-sample distance is 6 cm

cylindrically symmetric structure means that the layers of main chains in some way broke up or changed to a more fibrillar structure upon drawing. Besides the initial molecular order that may play a role, the reasons for this different behaviour must probably be sought in the less dense substitution of the polymers under investigation, when compared to PTA12HQ. An interpretation in terms of possible supramolecular structures will be discussed below.

Determination of the degree of orientation

The strongest equatorial reflection was used to determine the degree of orientation. The meridional scattering, which has been used in the literature to

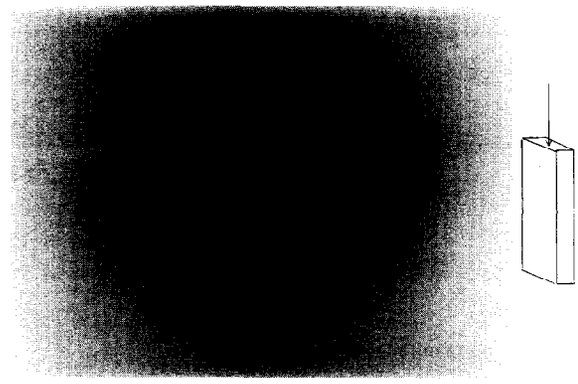

Figure 5 Flat-plate X-ray diffractogram of an oriented PES1.3/C6 film, taken with the beam parallel to the draw direction, as indicated on the figure

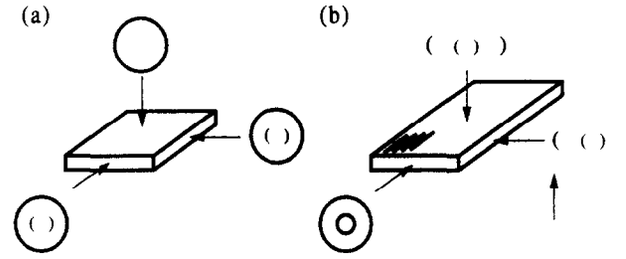

Figure 6 Schematic representation of X-ray diffractograms of the polyesters in the three principal directions, showing the change from (a) a layered structure in the as-cast film to (b) a fibre-symmetric structure in the drawn film

account for the local orientation[9], was too vague to be usable in our case. There are two important aspects in determining $\langle P_2 \rangle$ from the X-ray intensity profile: the subtraction of the background intensity and the assumption of the width of a perfectly aligned system. In the literature, the minimum intensity of the azimuthal scan has mostly been taken as a background value. The width of the perfectly aligned system has been taken as 0°, as described in the Experimental section. A larger 'perfect width' will result in slightly larger $\langle P_2 \rangle$ values.

Figure 7 shows the azimuthal intensity distributions at different draw ratios for PES1.3/C12. Relatively low intensity values at high azimuthal angles, ϕ, have a big influence on the determination of $\langle P_2 \rangle$, as was recognized by others[10–13]. In order to obtain an estimate of the contribution at large values of ϕ, the experimental profiles were fitted. As an illustration of the different fit functions, in *Figure 8* the experimental profile of the reflection of a PES3.3/C6 film with $\lambda = 2$ has been fitted by using a Gaussian function and a modified Lorentz function. From these and other distribution functions, it turned out that our experimental profiles could be described best by a modified Lorentz function[10,14], as follows:

$$I(\phi) = \frac{I(0)}{(1 + k\phi^2)^m}$$

with

$$k = \frac{2^{1/m} - 1}{(FWHM/2)^2} \qquad (2)$$

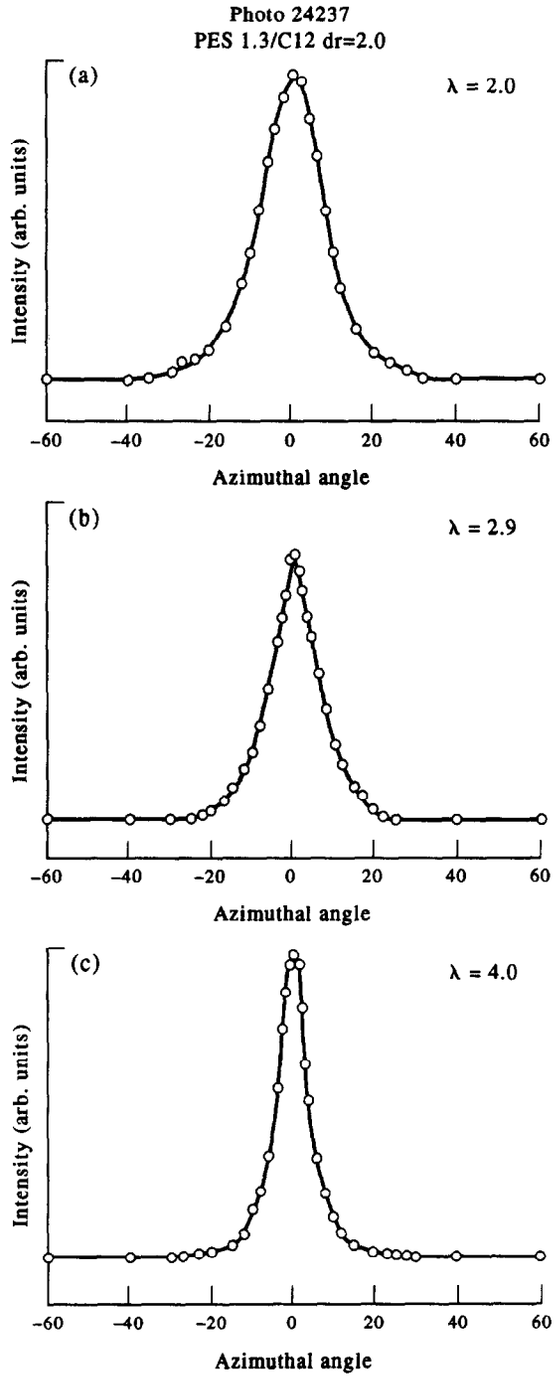

Figure 7 Azimuthal intensity distributions of the first equatorial reflection of PES1.3/C12 at different values of the draw ratio, λ: (a) 2.0; (b) 2.9; (c) 4.0. The X-ray beam was directed parallel to the film surface

In this equation, *FWHM* is the full-width-at-half-maximum of the peak, and m is a shape parameter. The function becomes Lorentzian when $m = 1$ and tends towards a Gaussian function as m goes to infinity. The measured profiles were fitted with the fixed, experimentally found value for the *FWHM*, while adjusting the parameter m, resulting in the value $m = 2$ for PES1.3/C12, and $m = 1.5$ for PES1.3/C6 and PES3.3/C6. Based on equation (1), the $\langle P_2 \rangle$ values were calculated in two different ways, i.e. one by using directly the experimental profile $I_{exp}(\phi)$, and the other by using the fitted profile $I_{fit}(\phi)$. The resulting orientation

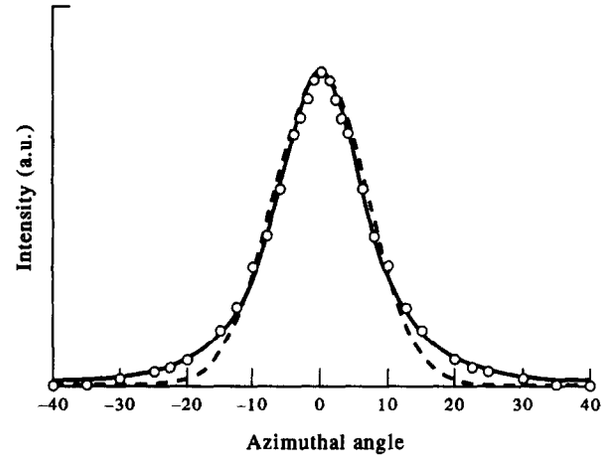

Figure 8 Comparison of functions fitted to the azimuthal intensity distribution of PES3.3/C6 at $\lambda = 2.0$: (O) experimental; (—) Lorentz function (see equation (2)); (– – –) Gaussian function

Table 3 $\langle P_2 \rangle$ values of drawn PES3.3/C6 films determined by using WAXD and Raman spectroscopy[15]

Draw ratio, λ	WAXD $\langle P_2 \rangle_{fit}$	WAXD $\langle P_2 \rangle_{exp}$	Raman $\langle P_2 \rangle$
1.5	–	–	0.19
2.0	0.77	0.90	0.42
2.2	0.78	0.91	–
2.3	0.80	0.87	–
2.4	–	–	0.54
2.5	0.78	0.91	–
2.6	–	–	0.56
2.7	0.81	0.93	–
2.8	–	–	0.66
2.9	0.79	0.94	–
3.0	0.87	0.94	–
3.1	0.89	0.95	0.68

parameters are $\langle P_2 \rangle_{exp}$ and $\langle P_2 \rangle_{fit}$, respectively. *Figure 9* shows $\langle P_2 \rangle_{exp}$ and $\langle P_2 \rangle_{fit}$ as a function of the draw ratio. By applying the fitting procedure, slightly lower $\langle P_2 \rangle$ values were obtained. The results show that at high concentrations, a very accurate value for $\langle P_2 \rangle$ cannot be obtained due to the 'background problem'. The figure also includes the *FWHM*, which is a directly measurable quantity. When using the second equatorial reflection instead of the first, slightly lower degrees of orientation were obtained, but the differences were very small.

Comparison of $\langle P_2 \rangle$ values obtained by WAXD and Raman spectroscopy

The degree of orientation in drawn PES3.3/C6 films was also established by Raman spectroscopy, which has been described in another publication[15]. The Raman shift at 1616 cm^{-1}, which was identified as the vibrational band of the phenylene ring in the C(1)–C(4) direction, was used to determine $\langle P_2 \rangle$ (and $\langle P_4 \rangle$). *Table 3* summarizes the results. The values obtained by using WAXD exhibit considerable differences when compared to the $\langle P_2 \rangle$ values obtained by Raman spectroscopy. These could not be ascribed to experimental uncertainties. It was assessed that the Raman method probes the average orientation of all phenylene groups in the

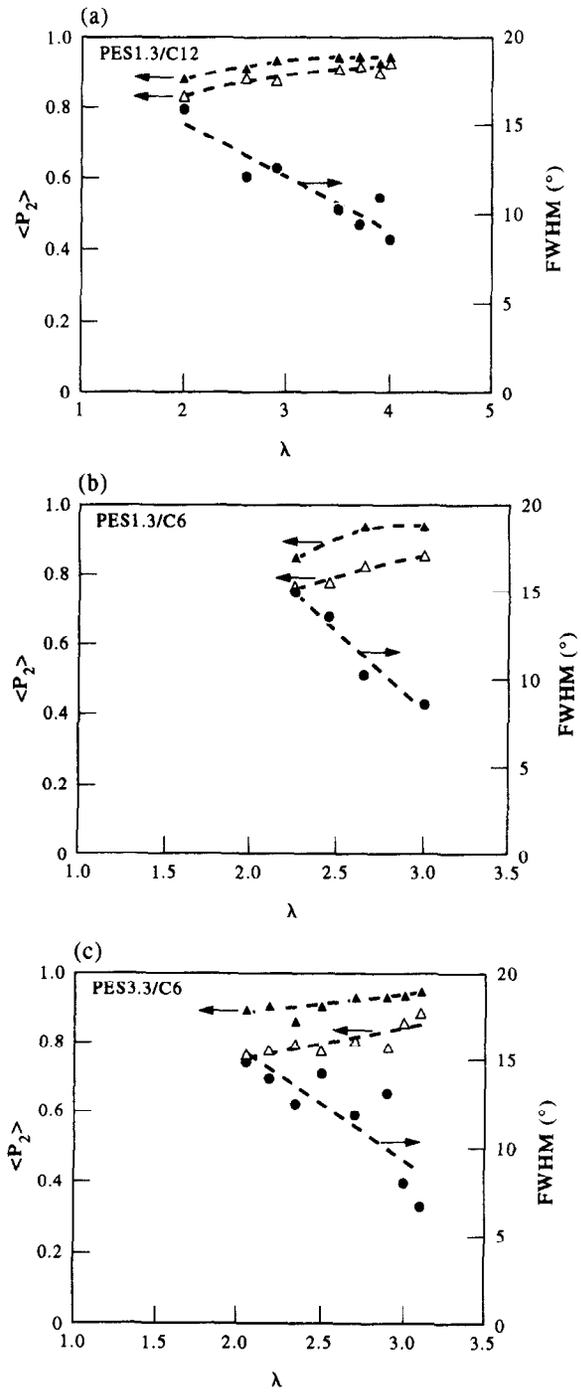

Figure 9 Orientation parameters $\langle P_2 \rangle$ and *FWHM* as a function of the draw ratio λ: (a) PES1.3/C12; (b) PES1.3/C6; and (c) PES3.3/C6. All figures: (▲) $\langle P_2 \rangle_{exp}$; (△) $\langle P_2 \rangle_{fit}$; (●) *FWHM*

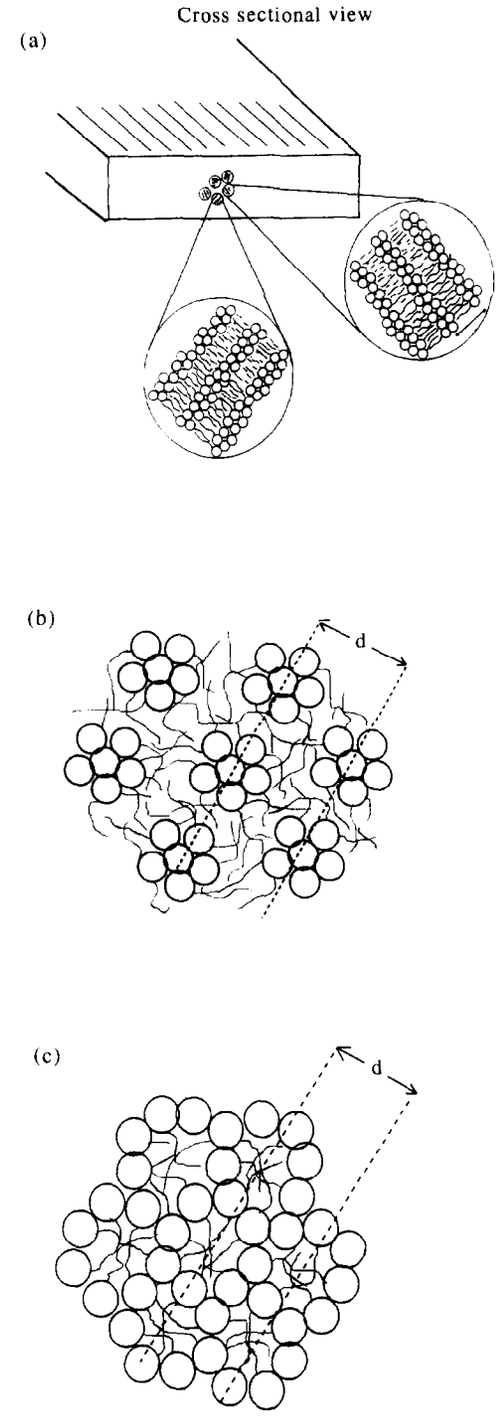

Figure 10 Schematic representations (cross-sections of the main chains) of possible drawn film structures based on WAXD and Raman data for PES3.3/C6: (a) layers of main chains, separated by layers of side chains; (b) clusters of main chains, surrounded by a continuous structure of side chains; (c) clusters of side chains, surrounded by a continuous structure of main chains

material, so this $\langle P_2 \rangle$ value reflects the orientation on a molecular level, which appears to be moderate; the meridional streaks in the X-ray diffractograms, which are said to give the *intra* chain scattering[9], are in line with these Raman results. The equatorial WAXD reflections, on the other hand, measure the orientation distribution of larger entities (layers or clusters of chains), so this reflects the orientation on a supramolecular level. Obviously, the orientation development of layers or clusters as a whole is much more effective than the orientation development of chains within these layers or clusters.

Possible morphologies of oriented films

Based on the results of the previous section, three possible morphologies of oriented films of this class of polyesters are proposed. The cross-sections of these structures perpendicular to the orientation direction are shown schematically in *Figure 10*. For a better understanding of the morphology, the side chains and the main chains can be compared with the two components of a block copolymer, which phase separate on a microscopic

scale[16]. In the first proposed structure, the main chains are arranged in layers, separated by the side chains, according to the structure in PTA12HQ[5]. The fibre symmetry of the drawn films, deduced from the axial X-ray recordings, can be explained by assuming domains, with different orientations of these layered structures. This model is visualized in *Figure 10a*. In the second possible structure (*Figure 10b*), the main chains form clusters (nanofibrils), which are surrounded by a continuous structure of the side chains. Each cluster consists of a number of main chains. The uniaxial symmetry is a natural consequence of this fibrillar structure, which was reported earlier for several other systems[17–19]. Using the experimental X-ray spacings, the structure can be brought into agreement with the experimental densities, with clusters consisting of five (PES1.3/C6 and PES3.3/C6) or seven (PES1.3/C12) main chains. There would be a strong indication for this type of fibrillar structure when the squared distance between the neighbouring fibrils increased linearly with the number n of methylene units in the side chain[18,19]. With our limited number of data points this correlation resulted in a negative intercept (at $n = 0$), which is not realistic. The third possible structure is shown in *Figure 10c*, and this is, in fact, the 'inverted' structure of *Figure 10b*. The clusters are now formed by the side chains, and are surrounded by a continuous structure of the main chains. This model is more in line with the ratio of main chains to side chains. It preserves the uniaxial symmetry, and can still explain the experimentally found X-ray reflections. The structure can be brought into agreement with the experimental densities of the three polyesters, with again five to seven main chains building up a cylinder around a side-chain cluster. The cross-sectional views of *Figures 10b* and *10c* are drawn in a hexagonal lattice, for the sake of clarity. In reality, these structures may be less ordered.

From the viewpoint of microphase-separated block copolymers[16], it may be considered plausible that PTA12HQ, which contains 61 wt% side chains, shows a layered structure, while PES1.3/C6, PES3.3/C6 and PES1.3/C12, which contain only 30, 38 and 46 wt% side chains, respectively, might be packed in an 'inverted fibrillar' structure.

The moderate degree of orientation determined by Raman spectroscopy can be explained by assuming that the individual main chains are not fully stretched. On the other hand, the order between the layers or fibrils can be very high, which explains the high degree of orientation determined by X-ray diffraction.

The mechanical properties will be different for the various structures shown in *Figure 10*. The highest tensile properties are expected for the structure in *Figure 10c*, because of the continuous structure of the main chains, which accounts for a good force transfer. On the other hand, the lowest tensile properties may be expected of the model in *Figure 10b*, because the continuous structure of the side chains accounts for a lower force transfer. The mechanical properties will be discussed in a subsequent paper[20].

Comparison of the orientation development with deformation models

Notwithstanding the uncertainties in determining the absolute value of $\langle P_2 \rangle$, it is clear that in the polymers under investigation in this work there is an extremely efficient development of orientation with draw ratio, which is, to our knowledge, the most efficient ever reported. It is interesting to compare this orientation development with the affine deformation model[21,22], which is known to describe the most efficient development of orientation for non-interacting rods by assuming a rotation of the rods only, without any shearing. The orientation development in this model is described by $\tan\theta' = \lambda^{-3/2}\tan\theta$, with θ and θ' the angle between a rod and the draw direction before and after drawing, respectively. The second moment of the orientation distribution, $\langle P_2 \rangle = 0.5(3\langle\cos^2\Theta\rangle - 1)$, is then given as a function of λ by the following equation:

$$\langle\cos^2\theta\rangle = \frac{\lambda^3}{\lambda^3 - 1} - \frac{\lambda^3}{(\lambda^3 - 1)^{3/2}}\arctan(\sqrt{\lambda^3 - 1}) \quad (3)$$

As an example, the experimental $\langle P_2 \rangle$ values for PES3.3/C6 are shown together with the affine model in *Figure 11*. The much higher values, compared to the model, indicate that the experimental orientation development is not described properly by this model. One reason for this could be that the deformation does not start from a 3-dimensional random structure, but rather from a 2-dimensional random structure. The deformation then takes place in a plane, and is described by $\tan\theta' = \lambda^{-2}\tan\theta$, giving rise to the 'two-dimensional orientation parameter', $\langle P_2 \rangle_{z-y}$, given by the following equation:

$$\langle\cos^2\theta\rangle_{z-y} = \frac{\lambda^4}{\lambda^4 - 1} - \frac{\lambda^4}{(\lambda^4 - 1)^{3/2}}\arctan(\sqrt{\lambda^4 - 1}) \quad (4)$$

We should refer to the resulting orientation parameter as $\langle P_2 \rangle_{z-y}$, because it only represents the orientation in the z–y plane[23]. The use of equation (4) leads to higher orientation parameters, compared to a three-dimensional deformation, at the same draw ratio (see *Figure 11*).

However, the 2-dimensional affine model also predicts lower $\langle P_2 \rangle$ values than the experimental ones. An important explanation for the high effectiveness when compared to the affine model may well be related to the fact that the latter model assumes individual rods with a large aspect (l/d) ratio. When units with a small aspect

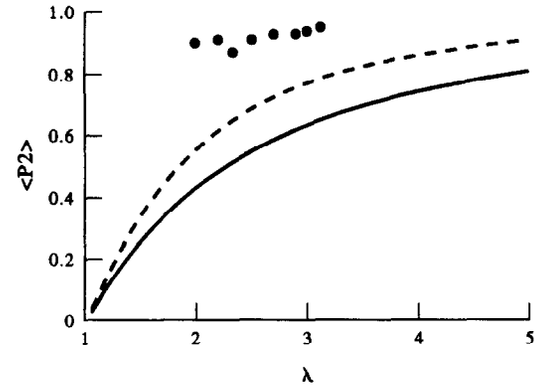

Figure 11 Development of $\langle P_2 \rangle$ with draw ratio: (●) $\langle P_2 \rangle_{exp}$ of PES3.3/C6 films; (—) 3-dimensional affine deformation model; (– – –) 2-dimensional affine deformation model

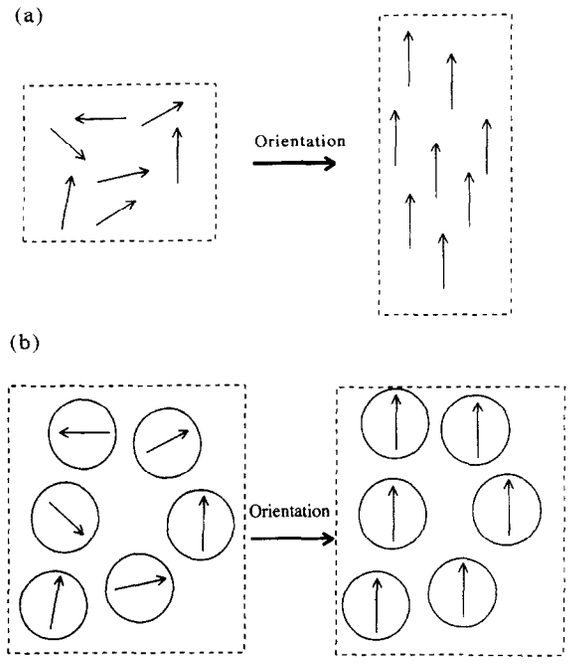

Figure 12 Schematic representations of orientation and elongation by: (a) rotation of thin rods; (b) rotation of spheres

ratio are involved, the orientation development may be much more effective. This could be the case when a number of chains or chain segments are clustered, and when these clusters are rotated. In the extreme case, for cubes or spheres, perfect orientation could be reached without any increase in length (see *Figure 12*), although in practice film drawing inevitably results in an increase in length. For these present polymers, it is very likely that the clusters of chains are associated with liquid crystalline domains. The apparently more effective orientation development in the films under investigation here when compared to the affine deformation model may be largely explained by the rotation of domains instead of individual chains.

If we assume that the clusters which are being oriented by drawing are the same as the units observed by WAXD, the dimensions of the units can be estimated via the radial widths of the equatorial and meridional reflections, by using the Scherrer equation[24]. The lateral dimensions of the units in a PES3.3/C6 film varied from ca. 45 Å (undrawn film) to 270 Å (at $\lambda = 3$), while the length of a unit was ca. 100 Å at $\lambda = 3$. When these units orient along the draw direction, the increase in length can be much smaller than the value predicted from the affine deformation model. In practice, part of the length increase will be due to shear, so the length increase associated with rotation is even smaller than that at $\lambda = 3$. The same can also be concluded for the PES1.3/C6 and PES1.3/C12 films.

CONCLUSIONS

Films of various polyesters containing terphenyl units in the main chain and hexyl or dodecyl side chains were investigated with respect to their structure and orientation development upon drawing. The as-cast polyester films showed a layered structure, with layers of the main chains extending parallel to the surface of the film. Upon drawing, this organization appeared to change to a fibre-symmetric structure, in contrast to the well studied polyester PTA12HQ.

The polyester films could be drawn up to a draw ratio of 3 to 4, showing a very effective orientation development. The differences in the orientation parameters obtained by WAXD and Raman spectroscopy were explained by the different molecular levels that these techniques can effectively investigate. Comparison of the orientation development with the affine deformation model and its two-dimensional version shows that the actual orientation development of the polymers investigated is much more efficient than that described by these models. The most probable explanation is the fact that the affine deformation model is based on non-interacting rigid-rods, while in the polyesters under investigation here the orientation develops by rotation of domains instead of individual chains, thus involving much smaller length increases.

ACKNOWLEDGEMENTS

The authors would like to thank Dr D. Vlassopoulos (FORTH-IESL, Greece) for useful discussions and for providing the orientation parameters obtained by Raman scattering, and Dr H. Fischer (Eindhoven University of Technology), Dr S. B. Damman and Dr F. P. M. Mercx for stimulating discussions and careful reading of the manuscript. The provision of the X-ray flat-film recordings by E. J. Sonneveld is greatly appreciated. This investigation was supported financially by the EC (Brite-Euram project BE 4490-90).

REFERENCES

1 Ballauff, M. and Schmidt, G. F. *Mol. Cryst. Liq. Cryst.* 1987, **147**, 163
2 Schrauwen, C., Pakula, T. and Wegner, G. *Makromol. Chem.* 1992, **193**, 11
3 Damman, S. B., Mercx, F. P. M. and Kootwijk-Damman, C. M. *Polymer* 1993, **34**, 1891
4 Damman, S. B., Mercx, F. P. M. and Lemstra, P. J. *Polymer* 1993, **34**, 2726
5 Damman, S. B. and Vroege, G. J. *Polymer* 1993, **34**, 2732
6 Tiesler, U., Pulina, T., Rehahn, M. and Ballauff, M. *Mol. Cryst. Liq. Cryst.* 1994, **243**, 299
7 Tiesler, U. *PhD Thesis*, University of Karlsruhe, 1994
8 Mitchell, G. R. in 'Comprehensive Polymer Science: Polymer Properties' (Eds G. Allen and J. C. Bevington), vol. 2, Pergamon, Oxford, 1989, Ch. 31, p. 701
9 Mitchell, G. R. and Windle, A. H. *Polymer* 1983, **24**, 1513
10 Lafrance, C. P., Debigaré, J. and Prud'homme, R. E. *J. Polym. Sci. Polym. Phys. Edn* 1993, **31**, 255
11 Northolt, M. G. *Polymer* 1980, **21**, 1199
12 Crevecoeur, G. and Groenincx, G. *Polym. Compos.* 1992, **13**, 244
13 Davidson, P., Petermann, D. and Levelut, A. M. *J. Phys. II (France)* 1994, **5**, 113
14 Murthy, N. S., Zero, K. and Minor, H. *Macromolecules* 1994, **27**, 1484
15 Voyatzis, G., Petekidis, G., Vlassopoulos, D., Kamitsos, E. and Bruggeman, A. *Macromolecules*, 1996, **29**, 2244
16 Quirk, R. P., Kinning, D. J. and Fetters, L. J. in 'Comprehensive Polymer Science: Special Polymers and Polymer Processing' (Eds G. Allen and J. C. Bevington), vol. 7, Pergamon, Oxford, 1989, Ch. 1, p. 14

17 Noël, C., Friedrich, C., Laupretre, F., Billard, J., Bosio, L. and Strazielle, C. *Polymer* 1984, **25**, 263
18 Fischer, H., Rötz, U., Lindau, J. and Kuschel, F. *Mol. Cryst. Liq. Cryst.* 1994, **238**, 147
19 Weber, P., Guillion, D., Skoulios, A. and Miller, R. D. *Liq. Cryst.* 1990, **8**, 825
20 Bruggeman, A. and Buijs, J. A. H. M. unpublished results
21 Kratky, O. *Kolloid Z. Z. Polym.* 1933, **64**, 213
22 Kuhn, W. and Grün, F. *Kolloid Z. Z. Polym.* 1942, **101**, 248
23 Pick, M., Lovell, R. and Windle, A. H. *Polymer* 1980, **21**, 1017
24 Alexander, L. E. 'X-Ray Diffraction Methods in Polymer Science', Wiley, New York, 1969, p. 423